The Astrophysical Journal, 627:1057–1065, 2005 July 10

NEAR-INFRARED SURFACE PROPERTIES OF THE TWO INTRINSICALLY BRIGHTEST MINOR PLANETS: (90377) SEDNA AND (90482) ORCUS[1]

Chadwick A. Trujillo
Gemini Observatory, Northern Operations Center, 670 North A'ohoku Place, Hilo, HI 96720; trujillo@gemini.edu

Michael E. Brown
California Institute of Technology, Division of Geological and Planetary Sciences, MS 150-21, Pasadena, CA 91125; mbrown@caltech.edu

David L. Rabinowitz
Physics Department, Yale Center for Astronomy and Astrophysics, Yale University, P.O. Box 208121, New Haven, CT 06520-8121; david.rabinowitz@yale.edu

and

Thomas R. Geballe
Gemini Observatory, Northern Operations Center, 670 North A'ohoku Place, Hilo, HI 96720; tgeballe@gemini.edu
Received 2004 March 26; accepted 2005 March 16

ABSTRACT

We present low-resolution *K*-band spectra taken at the Gemini 8 m telescope of (90377) Sedna and (90482) Orcus (provisional designations 2003 VB_{12} and 2004 DW, respectively), currently the two minor planets with the greatest absolute magnitudes (i.e., the two most reflective minor planets). We place crude limits on the surface composition of these two bodies using a Hapke model for a wide variety of assumed albedos. The unusual minor planet Sedna was discovered on UT 2003 November 14 at roughly 90 AU, with 1.6 times the heliocentric and perihelion distances of any other bound minor planet. It is the first solar system object discovered between the Kuiper Belt and the Oort Cloud and may represent a transition population between the two. The reflectance spectrum of Sedna appears largely featureless at the current signal-to-noise ratio, suggesting a surface likely to be highly processed by cosmic rays. For large-grain models (100 μm to 1 cm) we find that Sedna cannot have more than 70% surface coverage of water ice and cannot have more than 60% surface coverage of methane ice, to 3 σ confidence. Minor planet Orcus shows strong water ice absorption corresponding to less than a 50% surface fraction for grain models 25 μm and larger. Orcus cannot have more than 30% of its surface covered by large (100 mm to 1 cm) methane grains, to 3 σ confidence.

Subject headings: comets: general — Kuiper Belt — Oort Cloud — solar system: formation

1. INTRODUCTION

On UT 2003 November 14, the minor planet (90377) Sedna (provisional designation 2003 VB_{12}) was found as part of an ongoing survey for distant minor planets (Trujillo & Brown 2003; Brown et al. 2004a). As of 2005 May, with heliocentric distance 89.1 AU, Sedna is the most distant body bound to the Sun by about a factor of 1.6 (cf. comet 35P/Herschel-Rigollet at 55.7 AU, and Kuiper Belt object 2000 CR_{105} at 55.2 AU). It also has the largest perihelion distance (76 AU) of any solar system object by the same factor (cf. 1999 CL_{119} with 46.7 AU perihelion, and 2000 CR_{105} with 44.3 AU). The orbit of Sedna takes it from perihelion (near its current location) out to about 1000 AU. Formation scenarios for such an object are problematic; however, it is most likely to have originated in our solar system and represents an intermediate population between the Kuiper Belt and the Oort Cloud (Brown et al. 2004a and references therein). The orbit of (90482) Orcus (provisional designation 2004 DW) is more pedestrian, as it is in 3:2 resonance with Neptune, like Pluto. Sedna and Orcus currently are the two minor planets with the brightest absolute magnitude ($H = 1.6$ and 2.4, respectively), and they have both been discovered within the past 2 yr. Note that because of their extreme distances, although these are likely to be among the largest known minor planets, they are not the brightest by any means (Sedna is $V \sim 21$ and Orcus is $V \sim 19$), requiring the use of large telescopes for near-infrared investigations. Here we present near-infrared spectra of both of their surfaces and place limits on the presence of two volatiles, water ice and methane ice.

Due to its extreme distance, the surface of Sedna may be considerably more pristine than any Kuiper Belt object (KBO), or any closer object, which would be more susceptible to solar heating and collisions. The Galactic cosmic-ray environment of Sedna is likely to be similar to that found in the Kuiper Belt. Although large objects such as Sedna may have considerable radiogenic thermal processing deep in their interiors (McKinnon 2002), their exteriors are likely to be minimally processed by solar heating, with cosmic-ray processing being the dominant source of surface modification (Johnson et al. 1987). The temperature range due to solar heating of Sedna is 11–38 K between aphelion and perihelion, lower than any known KBO (typically $\sim$45 K). In the Kuiper Belt, collisions are thought to be rare between large bodies (Stern 1995) but possibly significant in terms of surface

[1] Based on observations obtained at the Gemini Observatory, which is operated by the Association of Universities for Research in Astronomy, Inc., under a cooperative agreement with the NSF on behalf of the Gemini partnership: the National Science Foundation (United States), the Particle Physics and Astronomy Research Council (United Kingdom), the National Research Council (Canada), CONICYT (Chile), the Australian Research Council (Australia), CNPq (Brazil), and CONICET (Argentina).

features, given the extreme color dispersion seen for KBO surfaces (Luu & Jewitt 1996). The collisional environment of Sedna is very different from that of the typical KBO. At aphelion, where an object on an eccentric orbit spends the most time, the space density of impactors and the likely velocity dispersion due to Keplerian motion are very roughly 10^4 and 10^2 times lower than in the Kuiper Belt, respectively. Although numerical simulations have produced collisions in the Oort Cloud (Stern 1988), these simulations involve a large number of very small ($\sim$1 km) bodies, a population that has not been observed in the Kuiper Belt and may be reduced from expected values (Kinoshita et al. 2003; Bernstein et al. 2003). Thus, Sedna has probably been minimally processed by solar heating and collisions, compared to the typical KBO.

The best constraints on the products of primitive volatiles bombarded by high-energy particles come from laboratory work, which suggests that simple volatiles expected from "pristine" objects (i.e., compositions unaltered since solar system formation) should produce more complex organic materials after undergoing bombardment by high-energy photons and particles (Moore et al. 1983; Johnson et al. 1987). Such bombardment causes the formation of complex organics such as Titan tholins, which are red throughout the visible to the J band (roughly 0.7 to 1.3 μm). Additional organics may also include primitive bitumens, which are rich in hydrocarbons and present transitions in the K band due to aromatic carbon-hydrogen (C—H) stretching, C=C stretching, and combinations of CH_2 and CH_3 stretching and symmetric bending (Moroz et al. 1998; Roush & Dalton 2002, 2004; McDonald et al. 1994). With additional bombardment, such compounds become more neutral and dark as they lose hydrogen and become chemically closer to carbon black (Johnson et al. 1987; Moroz et al. 2004). Additional compounds may also be present and become major components of primitive objects, as seen on Pholus, which shows methanol, water, olivine, and tholins (Cruikshank et al. 1998); Triton, with methane, nitrogen, carbon monoxide, and carbon dioxide (Cruikshank & Silvaggio 1979; Cruikshank et al. 1984, 1993; Quirico et al. 1999); Pluto, with nitrogen, methane, and carbon monoxide (Cruikshank et al. 1976; Owen et al. 1993; Nakamura et al. 2000); and KBOs, with water and possible metal-OH compounds (Brown et al. 1999; Jewitt & Luu 2001).

Water ice has been observed on several other KBOs and is a major constituent in comets. Methane ice is considerably more rare in the outer solar system, although it is thought that the largest, least thermally evolved objects, such as Sedna, may retain it. Recently, Fornasier et al. (2004) have reported a detection of water ice on the surface of Orcus, based on observations at the 3.56 m Telescopio Nazionale Galileo in La Palma. Their results for surface fraction covered by water ice are drawn from relatively lower signal-to-noise ratio near-infrared spectra as well as optical spectra. They have explored two possible models to explain their observations, both of which assume quite low albedos for the surface (4% and 10%). In this work, we place constraints on the presence of methane ice and water ice on Sedna and Orcus, using a simple Hapke model computed for a wide variety of possible surface albedos and grain diameters.

2. OBSERVATIONS

Reflectance spectra of Sedna and Orcus were collected on UT 2003 December 27 and 2004 April 2, respectively, from the Frederick C. Gillett Gemini Observatory Northern 8 m Telescope using the Near InfraRed Imager and spectrograph (NIRI; Hodapp et al. 2003) in f/6 mode ($0\farcs1165$ pixel^{-1}). Seeing for the two nights was stable throughout the observations at approximately $0\farcs6$ to $0\farcs7$ in R band, and $0\farcs3$ to $0\farcs4$ in K band. The Caltech Submillimeter Observatory (CSO) reported a 225 GHz optical depth of 4% to 7% (corresponding to the driest quartile of Mauna Kea conditions, approximately 1 to 1.7 mm precipitable water vapor) throughout the observations of Sedna, and 12% to 16% (corresponding to approximately 3 to 4 mm precipitable water vapor) for the observations of Orcus. In total, 110 minutes of on-source spectra were collected in K band over an air mass of 1.03 to 1.21 for Sedna, and 55 minutes were collected over an air mass of 1.11 to 1.20 for Orcus. Non-sidereal tracking rates of roughly $1''$ hr^{-1} and $2''$ hr^{-1} were used to track Sedna and Orcus, respectively. The $0\farcs7$ spectroscopic slit was imaged before, during, and after observation sequences to verify that the objects were properly centered in the slits. For Sedna, solar analog spectra of two G2 V stars were collected before (1.13 air masses, HD 377) and after (1.02 air masses, HD 42807) the science sequence, with less than 3% variation between the two observed spectra throughout the K band, except in regions affected by telluric water and carbon dioxide where less than 5% variation occurred ($<$1.96, 1.99–2.03, and 2.04–2.08 μm). For Orcus, a spectrum of solar analog HD 102196 collected at an air mass of 1.24 was used for calibration purposes. Photometric standards for Sedna were not taken on UT 2003 December 27, due to instrument failure shortly after collection of the science data and severe weather during subsequent nights. A rough photometric calibration was made using images of United Kingdom Infrared Telescope (UKIRT) Faint Standard FS 7 collected on UT 2003 December 6 and 7, the temporally closest available photometric standard, resulting in a K zero point of 23.36, consistent with previous telescope performance. Mirror resurfacing occurred before observations of Orcus, resulting in a fainter K zero point of 23.47 for Orcus. We find that the magnitudes of Sedna and Orcus were $K \approx 18.9$ and 18.0, respectively. Images of Sedna and Orcus were compared to field stars for the detection of possible companions. No evidence of elongation was apparent in the 8 minutes of $0\farcs31$ K acquisition images for Sedna and 3 minutes of $0\farcs46$ K acquisition images for Orcus.

3. DATA REDUCTION

Basic data reduction procedures were followed using the Interactive Data Language (IDL) produced by Research Systems, Inc. Processing included standard procedures for infrared observations, such as bad pixel replacement, pairwise sky subtraction, flat fielding, combination of science exposures into a single spectrum, wavelength calibration, and spectrum rectification. Final processing steps included spectrum extraction, residual sky subtraction, division by solar analog spectra to produce a reflectance spectrum, and averaging in the spectral direction to increase the signal-to-noise ratio at the expense of spectral resolution. Since NIRI produces spectra at much higher detector resolution (7.04×10^{-4} μm pixel^{-1}) than typical solid-state molecular transitions expected for outer solar system objects (0.025 μm), spectral data were binned to a resolution of 0.01 μm (14 pixels) by simple boxcar average. Errors in spectral flux were estimated for each wavelength range by measuring the standard error of the pixels incorporated into the wavelength range. This estimate is valid for broad features such as those observed but tends to overestimate errors in narrow-line regions, which were not apparent in our spectra. Overall, the spectrum of Sedna appears featureless. The spectrum of Orcus, in contrast, shows strong water ice absorption near 2.0 and 2.35 μm. The acquired reflectance spectra of

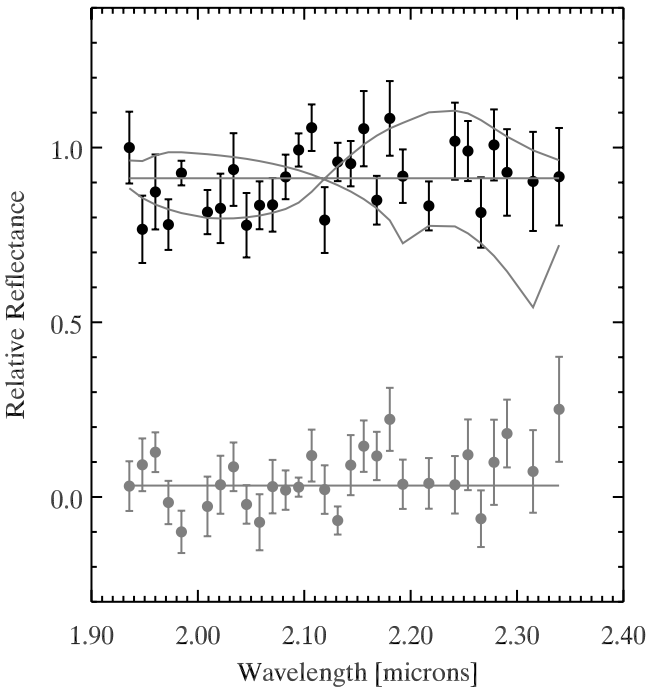

FIG. 1.—Relative reflectance spectrum of Sedna (*black circles*), and the spectrum of the nearby sky (*gray circles*). Gray curves are the model 3 σ upper limits to the surface fraction of water ice (*smooth gray line*) and methane ice (*jagged gray line*). Surface fractions that cause more absorption than the indicated lines are ruled out by our observations at the 3 σ level. The model shown is for 100 μm diameter particles. Spectrum error bars are computed from the reproducibility of the spectral data in each spectral point.

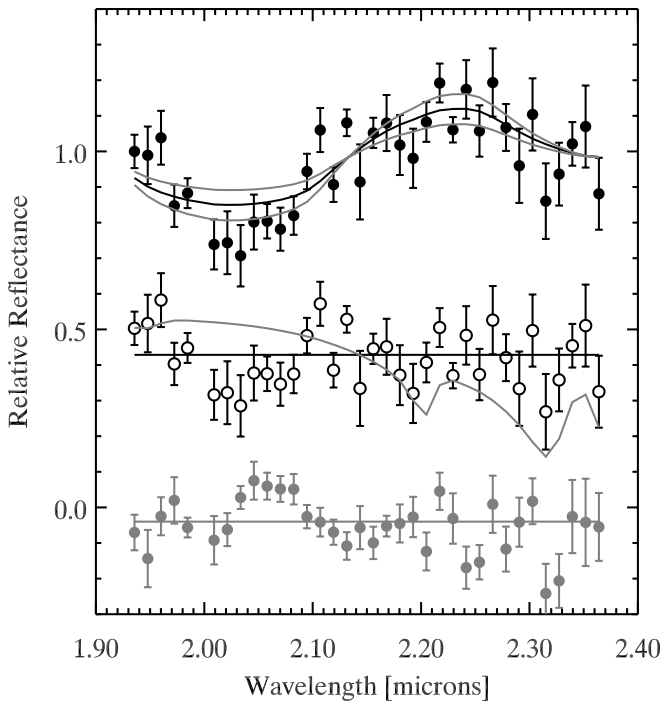

FIG. 2.—Relative reflectance spectrum of Orcus (*black filled circles*), and the spectrum of the nearby sky (*gray circles*). The top spectrum (*black filled circles*) shows the best-fit water-ice model and 1 σ limits on the best-fit model. The middle spectrum shows the residual model of Orcus after subtracting the best-fit water-ice model (*open circles, offset vertically for clarity*). The gray line on the middle spectrum illustrates the 3 σ methane ice model. Any greater amount of methane is ruled out by our observations. The model shown is for 100 μm diameter particles. Spectrum error bars are computed from the reproducibility of the spectral data in each spectral point.

Sedna and Orcus appear in Figures 1 and 2 with 100 μm grain diameter models overplotted.

4. HAPKE MODEL

Surface properties of the objects were explored using a bidirectional reflectance model (Hapke 1993). The reflectance spectra of Sedna and Orcus were compared to reflectance spectra generated using the Hapke model for methane and water ice. For Sedna, upper limits were placed on the surface fraction of volatile ices that could be present. For Orcus, which shows strong water ice absorption, the surface fraction of water ice and an upper limit to the fraction of the surface covered in methane ice were estimated. Because the albedos of Sedna and Orcus are not known, only relative reflectance spectra can be determined. Thus, abundances of compounds that are relatively featureless in the *K* band cannot be quantified, nor can compounds with very narrow features in the *K* band, which would not be seen in our low-resolution spectra. Compounds likely to exist on outer solar system surfaces that fall into these categories include carbon black and Titan tholins. The albedo of the body is considered a free parameter in our models, as the addition of substances such as carbon black can easily change the albedo without changing the normalized reflectance observed in this experiment.

Our model produces a geometric albedo (also known as physical albedo A_p) for each body, which is the ratio of a brightness of a body at a phase angle of $g = 0$ to the brightness of a Lambert disk of the same size and distance of the body observed at opposition. We model the physical albedo at zero phase angle, using the equation (Hapke 1993)

$$A_p \simeq r_0\left(\frac{1}{2}+\frac{1}{6}r_0\right)+\frac{w}{8}\{[1+B(0)]p(0)-1\}, \qquad (1)$$

where r_0 is the diffusive reflectance, $p(0)$ is the volume-angular-scattering function, w is the volume-single-scattering albedo, and $B(0)$ is the amplitude of the opposition effect. The quantity r_0 is related to w through the introduction of $\gamma = (1-w)^{1/2}$ such that $r_0 = (1-\gamma)/(1+\gamma)$. Under the assumption of large particles with only one substance present on the microscopic level, $w = Q_s$, where Q_s is the scattering efficiency excluding diffraction. We have considered only macroscopic mixtures of components, as the differences between models computed for microscopic and macroscopic mixing are too small to be significant in our low-resolution and low signal-to-noise ratio spectra. We use the internal scattering model to compute Q_s (Hapke 1993) from the real refractive index n, the imaginary refractive index k, and the absorption parameter α described below. We did not apply any adjustment to correct from the phase angle of observation ($g = 0\overset{\circ}{.}47$ and $0\overset{\circ}{.}93$ for Sedna and Orcus, respectively) to the zero phase angle modeled for the physical albedo. Correcting for phase angle would have made a very minor change to our computed surface fractions, <5% of the abundances computed for very deep absorptions such as those found near pure methane ice transitions. The opposition effect of known KBOs was considered in the context of the Hapke model, as it is an input parameter even when modeling zero phase angle as we did.

4.1. *The Opposition Effect*

Very little is known about the phase function of outer solar system bodies such as the KBOs. The most comprehensive study to date was that of Sheppard & Jewitt (2002), who found that the KBOs exhibited remarkable uniformity of opposition

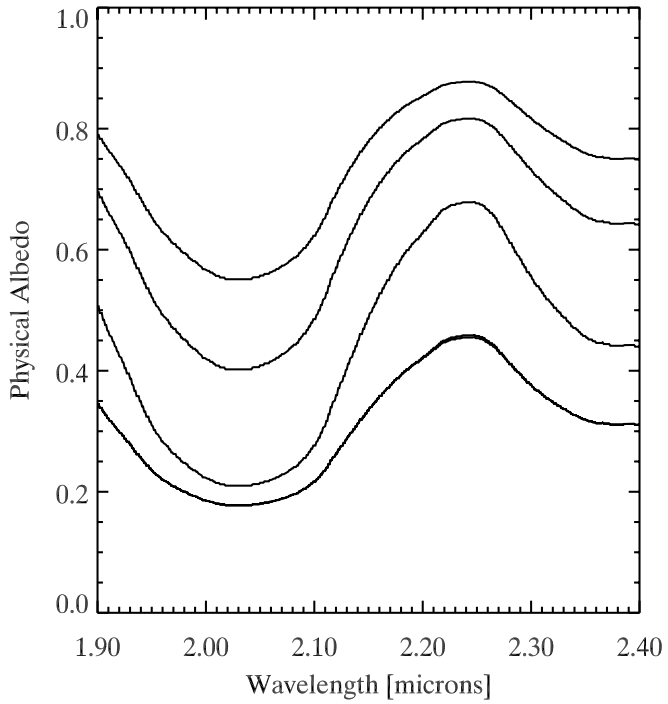

FIG. 3.—Physical albedo of a body composed of pure water ice, as computed by our Hapke model for (*top to bottom*) grain sizes 10 μm, 25 μm, 100 μm, 1 cm, and 10 cm. Note that the 1 and 10 cm models are nearly indistinguishable. See text for further details of the model.

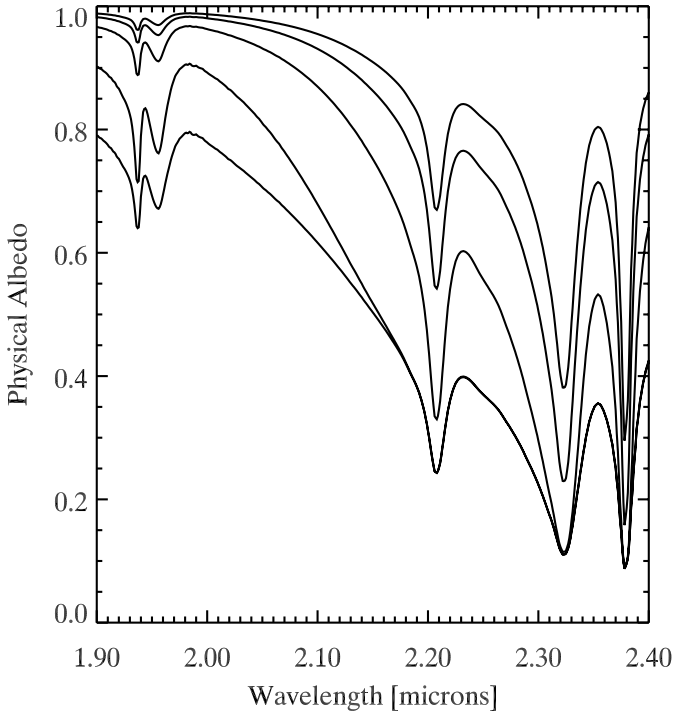

FIG. 4.—Physical albedo of a body composed of pure methane ice, as computed by our Hapke model for (*top to bottom*) grain sizes 10 μm, 25 μm, 100 μm, 1 cm, and 10 cm. See text for further details of the model.

surges within 2° of opposition. All of the seven KBOs studied became darker by ~0.15 mag per degree from opposition, a trend that was linear with phase angle up to 2°, the maximum phase of a distant KBO. This is a relatively large opposition effect compared to other solar system objects such as the asteroids (Bowell et al. 1989). Any believable reflectance model of KBO surfaces must reproduce this trend and in particular must reproduce the very strong Orcus phase function of ~0.20 mag per degree (Rabinowitz et al. 2004), which we have adopted in this work. We considered several different particle-angular-scattering functions, $p(g)$, of increasing complexity, as defined in Hapke (1993): a simple isotropic scattering function [$p(g) = 1$], a Lambert function, a Lommel-Seeliger function, and a double Henyey-Greenstein function with two free parameters. All of the functions were able to reproduce the phase function found by Sheppard & Jewitt (2002) with an appropriate choice of $B(0)$ and parameters of the various models. For all models, a very low density surface layer was required, with a filling factor of only $\phi \sim 5\%$, corresponding to an opposition surge half-width of about 1°. Such a low filling factor is consistent with "fluffy" material comprising the top visible layer of KBO surfaces. For the double Henyey-Greenstein function, values of $b = 0.2$ and $c = 1.0$ fit the phase function best and are typical of materials with a *high* density of internal scatterers within the particles, characteristic of natural ices with many inclusions and cracks. Henyey-Greenstein parameters consistent with a *low* density of internal scatterers fit the observed phase function poorly and were rejected. We chose the simplest Hapke grain model parameters that produced adequately steep opposition effects, namely isotropic scatterers [$p(g) = 1$] with $B(0) = 2.5$. This produced opposition effects of a similar magnitude to those found by Sheppard & Jewitt (2002) under a wide variety of assumed albedos. Our $B(0)$ assumption corresponds to a 20% increase in flux near opposition over the typical $B(0) = 1$ assumption used in other Hapke models. Grain size uncertainty exceeds opposition effect uncertainties in all model calculations.

4.2. *Grain Sizes*

We modeled a range of grain sizes, since the grain sizes of particles on Sedna and Orcus are not known. Recent models of Pluto and Charon used grain diameters of 75 μm to 1 cm (Cruikshank et al. 1997), and recent modeling of Triton used grain sizes of 100 μm to 9 cm (Quirico et al. 1999). We modeled spherical particles with diameters of 10 μm, 25 μm, 100 μm, 1 mm, and 1 cm, which span a wide range of absorption in the modeled reflectance spectra. These models are shown in Figures 3 and 4. The different grain size models change the overall albedo, but they do not significantly change the shape of the absorptions for water ice, and they only slightly change the shape of the methane bands at the low resolution observed. The grain sizes affect the amount of ice required to produce the observed absorption, as larger grains in general have much more absorption per unit area than smaller grains. Our relative reflectance model is generally most sensitive to grains of intermediate size, for which contrast between different wavelengths in the K band is greatest because absorption is strong but not yet saturating, particularly for methane. However, it should be noted that the contrast due to absorption in the K band is not a simple linear function of grain size, so the preceding statement is not strictly true in all cases.

4.3. *Optical Constants*

Optical constants used in the Hapke model were culled from the available literature in temperature ranges that are typical of outer solar system bodies (<40 K). If no such low-temperature laboratory results were available, higher temperature constants were used. For the water ice model, real indices of refraction were obtained from Warren (1984; 266 K), and wavelength-dependent absorption coefficients for hexagonal water ice at

20 K temperatures were found in Grundy & Schmitt (1998). For methane ice, the real refractive index was assumed to be uniformly 1.32 over the *K* band, consistent with the assumptions of Pearl et al. (1991). The wavelength-dependent absorption coefficient for methane at 30 K was found in Grundy et al. (2002). For both chemicals, the wavelength-dependent imaginary index of refraction k was estimated from the absorption coefficient $\alpha(\lambda)$ using the formula $k(\lambda) = \alpha(\lambda)\lambda/4\pi$, where λ is the wavelength of interest, as used in Quirico et al. (1999).

4.4. *The Neutral Absorber*

In our models, the overall *K*-band albedo of the body is treated as a free parameter, p. Only two components are used, that of either water ice or methane ice (depending on which is being fit), and that of an absorber neutral in the *K* band with an albedo chosen to produce the selected *K*-band albedo p. The albedo of the neutral absorber depends on the surface fraction f of the body covered with ice and the mean model *K*-band albedo p_m, as computed in the current ice model (Figs. 3 and 4). In algebraic terms, the neutral absorber has albedo $(p - fp_m)/(1 - f)$. Physical albedo models requiring neutral absorber albedos larger than unity were rejected. There was no specific chemical composition associated with the neutral absorber. However, laboratory tholins are mostly neutral in the *K* band and show a wide range of reflectances from 0.0 to 0.4 (Roush & Dalton 2004).

4.5. *Model Limitations*

The largest limitations to our models are the unknown *K*-band albedos of Sedna and Orcus. This is due primarily to the faintness of the targets in the submillimeter regime, which makes it difficult to obtain thermal observations. Typically, thermal observations can be combined with visible photometry to yield albedos, such as has been done for Varuna and (55565) 2002 AW_{197} (Jewitt et al. 2001; Margot et al. 2002). This, however, can only be done for a few of the largest bodies, and Sedna and Orcus have not yet been detected at thermal wavelengths (although upper limits on size have been placed on Sedna by Brown et al. 2004b). Because of the unknown *K*-band albedos, we have computed our surface reflectance models for a variety of assumed albedos. The second largest model limitation is that the typical diameters of the surface grains are unknown. Constraining grain sizes is quite difficult without very high signal-to-noise ratio spectra, a known albedo, and the presence of narrow absorptions. As mentioned previously, in all models, grains of different compositions were assumed to occupy different parts of the object disk; all Hapke modeling assumed homogeneous materials. There is an additional limitation to the observations presented here, namely that only one epoch of observations was conducted. True planet-wide abundances may depart from the analysis presented here if the surfaces of either Orcus or Sedna have large inhomogeneities on hemispherical scales.

5. (90377) SEDNA AND (90482) ORCUS

We use the apparently featureless near-infrared reflectance spectrum of Sedna to place upper limits on the surface fraction covered by water ice and methane ice under a wide variety of assumed albedos. We characterize the surface of Sedna with a Hapke model, as described above, with three free parameters. The first two free parameters are the assumed *K*-band albedo and the grain diameter. The third free parameter is the fraction of either water ice or methane ice. The best-fit model for each surface composition was determined by minimizing the χ^2 statistic. For Sedna, first water ice models were considered. Only the fraction of water ice was considered as a free parameter for a given grain size and *K*-band albedo. The χ^2 statistic was minimized for the selected grain size and *K*-band albedo (for all grain sizes and albedos, the reduced χ^2 was between 1.19 and 1.22). Since no absorption features were apparent at the noise level of the observed spectrum, our best-fit χ^2 was statistically equivalent to a zero water ice fraction. We estimated the 3 σ upper limit to the amount of water ice that could be present on Sedna by using an *F*-test (Bevington & Robinson 1992). In the *F*-test, the χ^2 computed for zero water ice was compared to the χ^2 computed from successively larger surface fractions of water ice. When the perturbations were so great that the *F*-test signaled a 3 σ statistical change, this point was marked as the 3 σ upper limit for water ice. This procedure was repeated for all grain sizes and all assumed *K*-band albedos, with results summarized in Figure 5. Results appear in their entirety in Table 1.

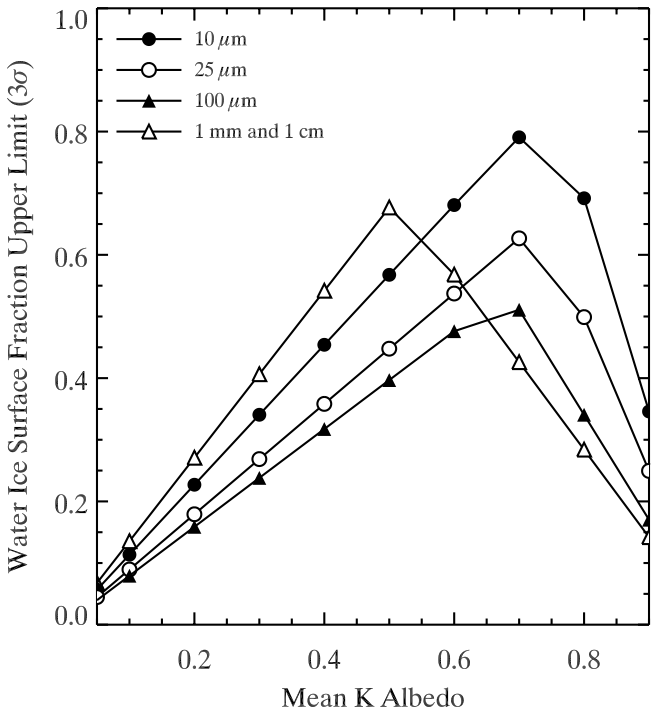

FIG. 5.—Upper limits (3 σ) to the surface fraction of water ice for Sedna under a variety of assumed mean albedos and grain diameters. To 3 σ confidence, the surface of Sedna must be covered by less than 70% water ice for grain diameters 25 μm or larger.

An identical procedure was performed for methane ice on Sedna, as no methane absorption was apparent either. Best-fit χ^2 models were statistically equal to zero methane ice fraction, as was true for the water ice case. The χ^2 for a model with zero methane ice (χ^2 was between 1.19 and 1.22 for all grain sizes and albedos) was compared to that of increasing fractions of methane ice until a 3 σ limit was indicated by an *F*-test. This procedure was repeated for all grain sizes and *K*-band albedos considered and is summarized in Figure 6 and Table 1. For grain diameters 25 μm or larger, and all albedo combinations, the surface fraction of water ice on Sedna must be less than 70%, or it would be detected in our observations at the greater than 3 σ significance level. Similarly, for methane ice, we find in Figure 6 that for moderate to large grains (diameters 100 μm or larger), the surface fraction of methane ice must be less than 60% for Sedna, or methane would have been detected in our observations at greater than 3 σ significance.

TABLE 1
(90377) Sedna

Grain Diameter (μm)	Mean K Albedo	Water Fraction Upper Limit (3 σ) (%)	Methane Fraction Upper Limit (3 σ) (%)
10	0.05	6	8
	0.10	11	16
	0.20	23	32
	0.30	34	48
	0.40	45	64
	0.50	57	80
	0.60	68	91
	0.70	79	96
	0.80	69[a]	98
	0.90	35[a]	84[a]
25	0.05	4	6
	0.10	9	11
	0.20	18	22
	0.30	27	33
	0.40	36	44
	0.50	45	55
	0.60	54	66
	0.70	63	76
	0.80	50[a]	85
	0.90	25[a]	59[a]
100	0.05	4	4
	0.10	8	7
	0.20	16	14
	0.30	24	21
	0.40	32	28
	0.50	40	35
	0.60	48	42
	0.70	51[a]	49
	0.80	34[a]	57
	0.90	17[a]	37[a]
1000	0.05	7	3
	0.10	14	6
	0.20	27	12
	0.30	41	18
	0.40	54	24
	0.50	68	30
	0.60	57[a]	36
	0.70	43[a]	42
	0.80	28[a]	47
	0.90	14[a]	24[a]
10,000	0.05	7	4
	0.10	14	8
	0.20	27	15
	0.30	41	23
	0.40	55	30
	0.50	68	38
	0.60	57[a]	46
	0.70	43[a]	53
	0.80	28[a]	43[a]
	0.90	14[a]	21[a]

Note.—Upper limits to surface fraction of water ice and methane ice on Sedna for a variety of grain sizes and mean K albedos.

[a] Upper limit is a physical limit; any higher fraction would require a mixing albedo greater than unity.

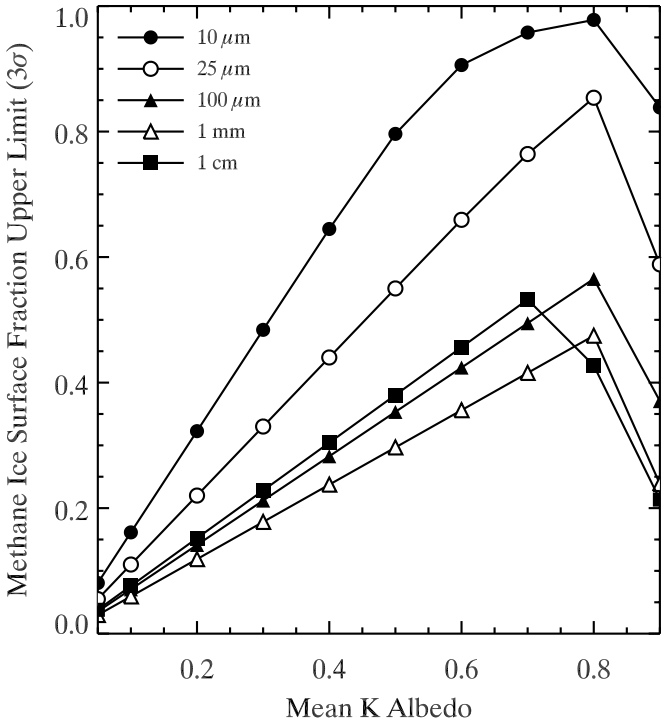

Fig. 6.—Upper limits (3 σ) to the surface fraction of methane ice for Sedna under a variety of assumed mean albedos and grain diameters. Assuming grain diameters 100 μm or larger, we find that to 3 σ confidence the surface of Sedna must be covered by less than 60% methane ice.

For Orcus a similar procedure was adopted, with minor modifications since water ice was apparent in the spectrum. Since water ice was detected, all water ice calculations estimate the 1 σ error bars on the detection rather than the 3 σ upper limits computed above for Sedna. The χ^2 statistic was minimized using the fraction of water ice as a free parameter for the selected grain size and K-band albedo (for all grain sizes and albedos, the reduced χ^2 was between 1.32 and 1.54). The reported 1 σ limits on the surface fraction of water ice was again computed by using an F-test. In the F-test, the best-fit χ^2 was compared to the χ^2 computed from perturbing the surface fraction of water ice from the best-fit values. When the perturbations were so great that the F-test signaled a >1 σ statistical change, this point was marked as the 1 σ error bar limit. This procedure was repeated for all grain sizes and all assumed K-band albedos, with results summarized in Figure 7 and displayed in their entirety in Table 2.

The 3 σ upper limits for methane ice were computed after subtracting the best-fit water ice model spectrum from Orcus. The residual spectrum was then fit with a methane ice model combined with a neutral absorber. As for Sedna, the surface fraction of methane required to produce the best-fit χ^2 did not deviate significantly from zero, so a neutral absorber was used as our best-fit spectrum (reduced χ^2 was between 1.23 and 1.54 depending on the grain size and K-band albedo assumed). The 3 σ upper limit on the amount of methane ice that could be present was estimated using the F-test. The fraction of methane ice was increased until the computed F-test comparing the new χ^2 to that of zero methane ice χ^2 showed a 3 σ deviation yielding our 3 σ upper limit for the amount of methane ice that could be on the surface of Orcus. Again, this procedure was repeated for all grain sizes and all assumed K-band albedos to produce Figure 8 and Table 2. Figure 8 indicates that methane ice must be restricted to less than 30% of the surface of Orcus unless grains are smaller than 100 μm. The best-fit models for water ice on the surface of Orcus show that less than 50% of the surface is covered with water ice if grains are 25 μm or larger (Fig. 7). Note that there is an upper limit to the K-band albedo for Orcus of about 0.7 for most grain models. Models with >0.7 K-band albedo would require a

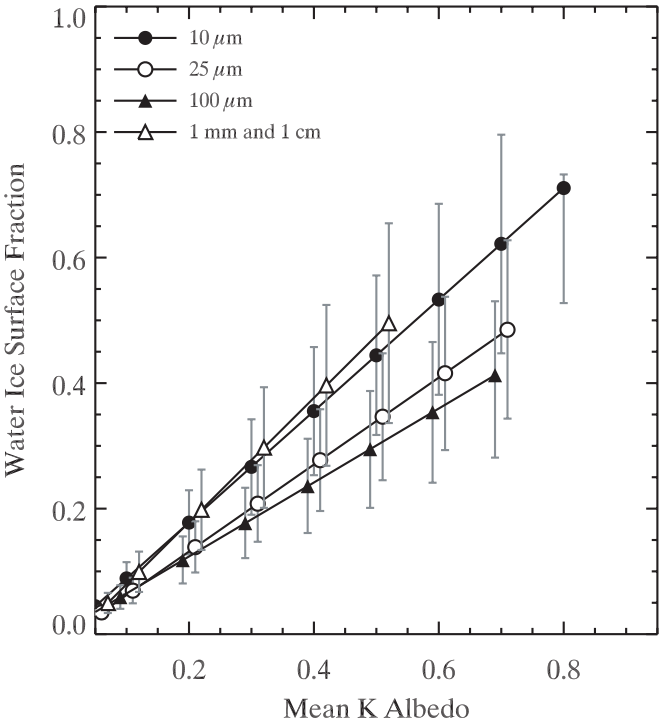

FIG. 7.—Best fit to the surface fraction of water ice for Orcus under a variety of assumed mean albedos and grain diameters (error bars are 1 σ). Points that do not appear and truncated error bars are not physically plausible, as they require a greater than unity albedo for the surface component that is not water ice. Unless grains are smaller than 25 μm, the surface of Orcus must be covered by less than 50% water ice.

mixing albedo greater than unity in the parts of Orcus not covered by water ice and are thus physically implausible.

6. COMPARISON TO KNOWN BODIES

Due to its size and very low temperature environment, it might be reasonable to expect the near-infrared observations of the surface of Sedna to be similar to that of either Pluto (dominated by methane ice absorption) or Charon (dominated by water ice absorption). Figure 5 rules out a Charon-like surface immediately, as Charon has a *K*-band albedo of ~20% and a surface fraction of water ice of 80%, assuming grains of diameter 100 μm (Roush et al. 1996). Figure 6 is not directly comparable to recent models of Pluto's methane (Cruikshank et al. 1997), as most Pluto models use methane dissolved in nitrogen, a model not considered in this work. However, a direct *F*-test comparing Sedna's spectrum to that of Pluto rules out the possibility that the surface of Sedna could be identical to that of Pluto at the 3 σ level.

The dissimilarity of Sedna's spectrum with both Pluto and Charon is somewhat unexpected, as these bodies are in principle similar to Sedna in terms of size and temperature (~40 K for Pluto/Charon and ~37 K for Sedna), although not in terms of color or origin. We note that the vast majority of Pluto's atmosphere is expected to be nitrogen, with only trace amounts of methane responsible for most of the near-infrared color (Cruikshank et al. 1997). Thus, although the spectrum of Sedna may be dissimilar to Pluto's, this difference could be primarily due to the methane abundance, since the nitrogen fraction on Sedna is unknown.

Pholus is a prime candidate for a possible compositional analog for Sedna. The surfaces of Pholus (one of the reddest in the solar system) and Sedna are similar in color in the visible (Rabinowitz et al. 2004). The Pholus model is consistent with the observed Sedna surface at the signal-to-noise ratio collected, and the water ice fraction observed on Pholus (15% for a 10 μm model) is well within the limits for Sedna (Cruikshank et al. 1998). Recently, Brown et al. (2004b) reported the detection of tholins on Sedna, consistent with a Pholus-like composition. Such tholins could not have been detected in our *K*-band spectra alone.

TABLE 2
(90482) ORCUS

Grain Diameter (μm)	Mean *K* Albedo	Water Fraction (1 σ Errors) (%)	Methane Fraction Upper Limit (3 σ) (%)
10	0.05	4^{+1}_{-1}	14
	0.10	9^{+3}_{-3}	26
	0.20	18^{+5}_{-5}	47
	0.30	27^{+8}_{-8}	61
	0.40	36^{+10}_{-10}	62
	0.50	44^{+13}_{-13}	55
	0.60	53^{+15}_{-15}	46
	0.70	62^{+17}_{-17}	38
	0.80	71^{+2}_{-18} [a]	29
	0.90	... [b]	... [b]
25	0.05	3^{+1}_{-1}	6
	0.10	7^{+2}_{-2}	11
	0.20	14^{+4}_{-4}	21
	0.30	21^{+6}_{-6}	29
	0.40	28^{+8}_{-8}	35
	0.50	35^{+10}_{-10}	40
	0.60	42^{+12}_{-12}	43
	0.70	49^{+14}_{-14}	43
	0.80	... [b]	... [b]
	0.90	... [b]	... [b]
100	0.05	3^{+1}_{-1}	3
	0.10	6^{+2}_{-2}	6
	0.20	12^{+4}_{-4}	12
	0.30	18^{+6}_{-6}	16
	0.40	24^{+8}_{-7}	20
	0.50	29^{+9}_{-9}	23
	0.60	35^{+11}_{-11}	26
	0.70	41^{+12}_{-13} [a]	27
	0.80	... [b]	... [b]
	0.90	... [b]	... [b]
1000	0.05	5^{+2}_{-2}	3
	0.10	10^{+3}_{-3}	6
	0.20	20^{+6}_{-6}	11
	0.30	30^{+10}_{-10}	14
	0.40	40^{+13}_{-13}	16
	0.50	50^{+16}_{-16}	17
	0.60	... [b]	... [b]
	0.70	... [b]	... [b]
	0.80	... [b]	... [b]
	0.90	... [b]	... [b]
10,000	0.05	5^{+2}_{-2}	4
	0.10	10^{+3}_{-3}	7
	0.20	20^{+6}_{-6}	13
	0.30	30^{+10}_{-10}	17
	0.40	40^{+13}_{-13}	20
	0.50	50^{+16}_{-16}	21
	0.60	... [b]	... [b]
	0.70	... [b]	... [b]
	0.80	... [b]	... [b]
	0.90	... [b]	... [b]

NOTE.—Upper limits to surface fraction of water ice and methane ice on Orcus for a variety of grain sizes and mean *K* albedos.

[a] Upper limit is a physical limit; any higher fraction would require a mixing albedo greater than unity.

[b] Best fit for the fraction of water ice requires a mixing albedo greater than unity and is omitted.

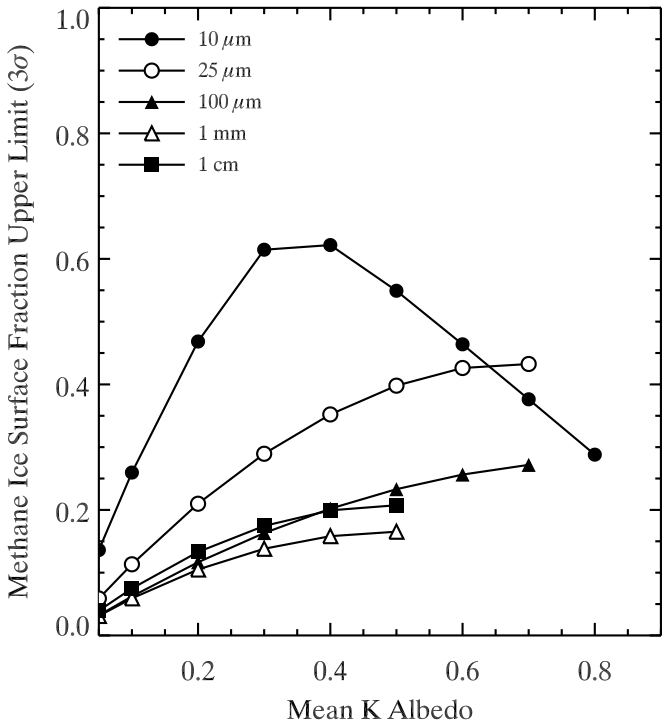

FIG. 8.—Upper limits (3 σ) to the surface fraction of methane ice for Orcus under a variety of assumed mean albedos and grain diameters after subtraction of the best-fit water-ice spectrum. Points that do not appear are not physically plausible, as they require a greater than unity albedo for the non–water ice surface components. For all models with grains >25 μm, the surface of Orcus must have less than 30% area coverage of methane ice.

The water ice observed on Orcus exists in moderate amounts. Assuming an albedo of roughly 20% to 40% in the *K* band, such as that found on Charon (20%) and Pluto (30%), we estimate that the surface of Orcus likely has between 15% and 30% water ice coverage, depending on the size of the grains involved. This is significantly less coverage than is found on Charon (80%; Roush et al. 1996) but is similar to the amount found on Triton (40%; Cruikshank et al. 2000). Since we find that the surface of Orcus cannot be entirely composed of water ice, it is possible that future work on Orcus may uncover more chemical components.

Although we have quantified the surface fraction of ices for model *K*-band albedos between 0.05 and 1.0 for completeness, a smaller possible range of albedos is more probable, given our current knowledge of outer solar system bodies. The icy Galilean satellites, for instance, have among the largest amounts of water ice observed in the solar system, yet they have *K*-band albedos between 0.25 and 0.35 outside water absorption bands, as measured by the *Cassini* Visual and Infrared Mapping Spectrometer (VIMS) under a variety of phase angles (Brown et al. 2003). One effect that may artificially increase the physical albedo of a KBO over that of the Galilean satellites is that KBOs are always observed near opposition, due to their extreme distances. However, even on icy Europa, the opposition surge is found to increase the flux by about 40% in the *K* band (Simonelli & Buratti 2004). Combining the expected opposition surge for an icy body (0.40) and reasonable albedos for well-studied icy bodies (0.25–0.35), we expect the upper limit for the *K*-band albedos to be about 0.50. Future works will undoubtedly test this further for both Sedna and Orcus. In any case, models have been run for high *K*-band albedos, but we believe that the results of the 0.5 or less models are the most physically relevant.

Using this stricter 0.5 albedo criterion for the possible range of albedos revises the results listed in the previous section only slightly. For Sedna, less than 40% of the surface can be covered with methane ice to 3 σ, while the water ice results are unchanged. For Orcus, the water ice model with maximum surface fraction shows 50% $\pm$ 16% water ice for all grain sizes, and there is no change to the methane ice results.

7. SUMMARY AND FUTURE WORK

We have obtained the near-infrared spectrum of Sedna and Orcus using the Gemini 8 m telescope. The spectrum of Sedna is featureless and consistent with other solar system objects with low to moderate absorptions in the *K* band. Compositions such as those of Pluto and Charon, which are dominated by very strong methane ice and water ice absorption, respectively, can be ruled out with greater than 3 σ confidence. No evidence of a companion was found in the 0.″31 *K*-band images for Sedna. Combining these data with observations in the visible (Rabinowitz et al. 2004) suggests that Sedna has a surface color similar to that of Pholus in the visible, presumably due to Titan tholin-like compounds, and has moderate, if any, absorption bands in the *K* region.

The surface of Orcus is considerably easier to characterize than that of Sedna, due to its brightness and the presence of moderate water ice features at 2 and 2.4 μm. No binary was seen in the 0.″46 *K*-band images for Orcus. Using the Hapke models we have produced, we can place crude constraints on the surface of the bodies studied. Specifically, we find the following:

1. To 3 σ confidence, the surface of Sedna cannot be covered by more than 70% water ice under most grain models and albedo combinations studied.
2. Assuming moderate to large grain models (diameters 100 μm or larger), the surface of Sedna cannot be covered by more than 60% methane ice to 3 σ confidence.
3. Unless grain diameters on Orcus are smaller than 25 μm, the surface of Orcus cannot be covered by more than 30% methane ice.
4. The best-fit models for grain diameters of 25 μm and larger suggest that the water ice surface fraction on Orcus is less than 50%. The maximum best-fit surface fraction of water ice is 50% $\pm$ 16%.
5. When the albedos of Sedna and Orcus are measured, the above results will be significantly more constrained, as only one albedo model need be considered.
6. Very low density grain models with filling factors of $\sim$5% are required to reproduce the strong opposition effect observed for KBOs with our Hapke model.

For both bodies, considerably more observations and analyses are needed. Constraining the albedos of the bodies would place strong limits on the surface fraction covered by water ice and methane ice, even given the fact that the grain sizes on the surfaces are unknown. Additionally, in this work, each object was observed at a single epoch. Once the rotation parameters of the bodies are known, it would be prudent to observe each of these bodies through a complete rotation as well as to consider additional chemical components as they become evident in higher signal-to-noise ratio spectra.

We thank C. M. Mountain for granting Director's Discretionary time for this project under Gemini program IDs GN-2003B-DD-3 and GN-2004A-DD-4. Alan Hatakeyama's support at the telescope was greatly appreciated. Operations at the telescope were greatly aided with the help of Simon Chan. Joe Jensen provided helpful input into constructing the observation sequence.

REFERENCES

Bernstein, G. M., Allen, R. L., Brown, M. E., Holman, M. J., Malhotra, R., & Trilling, D. E. 2003, BAAS, 35, 49.03
Bevington, P. R., & Robinson, D. K. 1992, in Data Reduction and Error Analysis for the Physical Sciences (2nd ed.; New York: McGraw-Hill), 205
Bowell, E., Hapke, B., Domingue, D., Lumme, K., Peltoniemi, J., & Harris, A. W. 1989, in Asteroids II, ed. R. P. Binzel, T. Gehrels, & M. S. Matthews (Tucson: Univ. Arizona Press), 524
Brown, M. E., Trujillo, C., & Rabinowitz, D. 2004a, ApJ, 617, 645
Brown, M. E., Trujillo, C. A., Rabinowitz, D., Stansberry, J., Bertoldi, F., & Koresko, C. D. 2004b, BAAS, 36, 03.01
Brown, R. H., Cruikshank, D. P., & Pendleton, Y. 1999, ApJ, 519, L101
Brown, R. H., et al. 2003, Icarus, 164, 461
Cruikshank, D. P., Brown, R. H., & Clark, R. N. 1984, Icarus, 58, 293
Cruikshank, D. P., Pilcher, C. B., & Morrison, D. 1976, Science, 194, 835
Cruikshank, D. P., Roush, T. L., Moore, J. M., Sykes, M., Owen, T. C., Bartholomew, M. J., Brown, R. H., & Tryka, K. A. 1997, in Pluto and Charon, ed. S. A. Stern & D. J. Tholen (Tucson: Univ. Arizona Press), 221
Cruikshank, D. P., Roush, T. L., Owen, T. C., Geballe, T. R., de Bergh, C., Schmitt, B., Brown, R. H., & Bartholomew, M. J. 1993, Science, 261, 742
Cruikshank, D. P., & Silvaggio, P. M. 1979, ApJ, 233, 1016
Cruikshank, D. P., et al. 1998, Icarus, 135, 389
———. 2000, Icarus, 147, 309
Fornasier, S., Dotto, E., Barucci, M. A., & Barbieri, C. 2004, A&A, 422, L43
Grundy, W. M., & Schmitt, B. 1998, J. Geophys. Res., 103, 25809
Grundy, W. M., Schmitt, B., & Quirico, E. 2002, Icarus, 155, 486
Hapke, B. 1993, Theory of Reflectance and Emittance Spectroscopy (Cambridge: Cambridge Univ. Press)
Hodapp, K. W., et al. 2003, PASP, 115, 1388
Jewitt, D., Aussel, H., & Evans, A. 2001, Nature, 411, 446
Jewitt, D. C., & Luu, J. X. 2001, AJ, 122, 2099
Johnson, R. E., Cooper, J. F., Lanzerotti, L. J., & Strazzulla, G. 1987, A&A, 187, 889
Kinoshita, D., Watanabe, J., Yamamoto, N., Fuse, T., Miyasaka, S., Muroi, K., & Tsai, A. 2003, in IAU Joint Discussion 19, Physical Properties and Morphology of Small Solar System Bodies, 47
Luu, J., & Jewitt, D. 1996, AJ, 112, 2310
Margot, J. L., Trujillo, C., Brown, M. E., & Bertoldi, F. 2002, BAAS, 34, 871
McDonald, G. D., Thompson, W. R., Heinrich, M., Khare, B. N., & Sagan, C. 1994, Icarus, 108, 137
McKinnon, W. B. 2002, in Proc. Asteroids, Comets, and Meteors (ESA SP-500; Noordwijk: ESA), 29
Moore, M. H., Donn, B., Khanna, R., & A'Hearn, M. F. 1983, Icarus, 54, 388
Moroz, L., Baratta, G., Strazzulla, G., Starukhina, L., Dotto, E., Barucci, M. A., Arnold, G., & Distefano, E. 2004, Icarus, 170, 214
Moroz, L. V., Arnold, G., Korochantsev, A. V., & Wasch, R. 1998, Icarus, 134, 253
Nakamura, R., et al. 2000, PASJ, 52, 551
Owen, T. C., et al. 1993, Science, 261, 745
Pearl, J., Ngoh, M., Ospina, M., & Khanna, R. 1991, J. Geophys. Res., 96, 17477
Quirico, E., Doute, S., Schmitt, B., de Bergh, C., Cruikshank, D. P., Owen, T. C., Geballe, T. R., & Roush, T. L. 1999, Icarus, 139, 159
Rabinowitz, D., Tourtellotte, S., & Schaefer, B. 2004, BAAS, 36, 03.02
Roush, T. L., Cruikshank, D. P., Pollack, J. B., Young, E. F., & Bartholomew, M. J. 1996, Icarus, 119, 214
Roush, T. L., & Dalton, J. B. 2004, Icarus, 168, 158
Roush, T. R., & Dalton, J. B. 2002, in 33rd Annual Lunar and Planetary Science Conference Abstracts (Houston: LPI), 1525
Sheppard, S. S., & Jewitt, D. C. 2002, AJ, 124, 1757
Simonelli, D. P., & Buratti, B. J. 2004, Icarus, 172, 149
Stern, S. A. 1988, Icarus, 73, 499
———. 1995, AJ, 110, 856
Trujillo, C. A., & Brown, M. E. 2003, Earth Moon Planets, 92, 99
Warren, S. G. 1984, Appl. Opt., 23, 1206